Comparing Planetary Helicopter Brownout Observations with Numerical Predictions for Ingenuity

Denis-Gabriel Caprace*, Ethan Baker†, Patricia Ventura Diaz‡, Seokkwan Yoon§
NASA Ames Research Center
Moffett Field, CA, USA

Ingenuity is considered the Martian equivalent of the Wright Flyer. Its sustained flights on Mars proved that non-terrestrial powered flight is possible, even on planets with thin atmospheres. However, Ingenuity was small and carried no payload. Future planetary rotorcraft will be bigger and heavier to accomplish new scientific and exploratory goals. On dusty planets, the associated increase in rotor thrust poses a potential challenge well known to helicopter pilots who have flown in desert environments: dust clouds forming during take-off and landing due to rotor wash, referred to as brownout. This work evaluates the effectiveness of existing numerical simulation models in predicting the severity of this phenomenon for planetary rotorcraft. We compare the output of a CFD-based dust mobilization model with data recently gathered using image processing techniques of Ingenuity's flights. The simulation results suggest that the sensitivity of the wall friction velocity to the rotorcraft height may be lower than previously assessed. We further evaluate the sensitivity of the total mass of mobilized dust to other model parameters such as the sandblasting efficiency and the saltation threshold velocity. Finally, we discuss the limitations of this comparison due to uncertainty in both the observation and the numerical model.

I. Nomenclature

α	=	Sandblasting efficiency [$\mathrm{m^{-1}}$]
b	=	Inter rotor distance [m]
d	=	Diameter of saltating particle [m]
Δx	=	Mesh resolution [m]
F	=	Flux of mobilized dust normal to the ground [$\mathrm{g\,m^{-2}\,s^{-1}}$]
g	=	Gravity acceleration [$\mathrm{m\,s^{-2}}$]
h	=	Height above the ground calculated as the distance between the ground and the bottom rotor plane [m]
Q	=	Saltation mass flux parallel to the ground [$\mathrm{g\,m^{-1}\,s^{-1}}$]
R	=	Rotor radius [m]
ρ	=	Ambient density [$\mathrm{kg\,m^{-3}}$]
ρ_s	=	Density of a solid particle [$\mathrm{kg\,m^{-3}}$]
ρ_p	=	Density of particulate matter in the flow [$\mathrm{g\,m^{-3}}$]
θ_0	=	Blade pitch angle [°]
ν	=	Fluid kinematic viscosity [$\mathrm{m^2\,s^{-1}}$]
$\mathbf{u}$	=	Flow velocity [$\mathrm{m\,s^{-1}}$]
$\mathbf{u}_\mathrm{g}$	=	Particle fallout velocity due to gravity [$\mathrm{m\,s^{-1}}$]
u_it	=	Impact threshold velocity [$\mathrm{m\,s^{-1}}$]
u_ft	=	Fluid threshold velocity [$\mathrm{m\,s^{-1}}$]
w	=	Far field rotor induced velocity [$\mathrm{m\,s^{-1}}$]
Ω	=	Rotor rotational speed [$\mathrm{s^{-1}}$]

*Oak Ridge Associated Universities, NASA Postdoctoral Program fellow, AIAA member. Corresponding author: denis-gabriel.caprace@nasa.gov
†Intern, Computational Physics Branch.
‡Science and Technology Corporation, AIAA member.
§NASA Advanced Supercomputing Division.

II. Introduction

Planetary exploration with aerial vehicles, as improbable as it seemed only a few decades ago, has now proven to be a formidable opportunity to increase the yield of science missions to extraterrestrial worlds [1]. Ingenuity —the small helicopter deployed on Mars by NASA's Perseverance rover and first ever man-made device to achieve powered flight outside Earth atmosphere (Fig. 1)— has demonstrated the feasibility of operating a rotorcraft on another planet [2]. This opens the door to many future missions to Mars and other frontiers with rotorcraft of increasing size and complexity.

Fig. 1 Ingenuity on the surface of Mars.

Operating a rotorcraft in dusty environments presents a number of challenges and risks that must be assessed during the design of the vehicle. In particular, the phenomenon of brownout can occur when the rotorcraft hovers close to the ground in a region where it is said to be "in ground effect" (IGE). This region is characterized by an unsteady and complex rotor-generated airflow. In a dusty environment, this flow interacts with the particulate matter lying at the surface. Given certain circumstances (driven by the magnitude of the flow velocity, the fluid and particle properties, gravity, etc.), particles can get entrained into the flow, creating a cloud of "dust" that can jeopardize safe operations and degrade the longevity of systems.

On Earth, brownout can put helicopter operations at risk by blocking the pilot's visibility or reducing situational awareness. This naturally occurs during take-off and landing, where, coincidentally, precise control is most vital. A similar danger exists for planetary rotorcraft which would use vision-based sensors or instruments. Since dust mobilization usually increases with the rotor disk loading (and, generally speaking, with the vehicle mass) [3], this topic needs to be accounted for in the design of increasingly heavy planetary aerial vehicles that will carry payloads and perform more complex scientific missions [4, 5]. Additional areas of concern related to brownout are dust erosion and/or accumulation which, for example, could perturb the functioning of critical mechanisms (such as rotor swashplates) or cause a premature drop in the performance of solar arrays [6]. Another potential hazard comes from the possibility of energetic discharge of particles electrically charged by impingement of suspended material on the rotors [7]. The risks associated with each of these aspects must be carefully assessed for future flights on Mars and beyond. Notably, the Dragonfly mission to Titan is expected to operate in a regime where brownout could be a factor, which has prompted a number of investigations [8, 9]. However, obtaining reliable predictions of the brownout phenomenon is challenging due to the complex nature of the problem: there is significant uncertainty in the processes involved which results in modeling and parameterization errors. Thus, verification is necessary to increase confidence in available models and their applicability in non-terrestrial environments.

Substantial work has been done on numerical modeling of helicopter brownout. In addition to analytical models, simulation tools have been developed to produce more accurate results (see, e.g., [10–13] and references therein). The present work relies on a numerical approach that, as far as dust modeling is concerned, presents strong similarity with these previous works. A vortex particle-mesh (VPM) method is employed to simulate the flow around Ingenuity. This computational fluid dynamics (CFD) method is a medium-fidelity tool that enables long rotorcraft simulations at an affordable computational cost, a critical feature that further enables parametric analyses. The CFD code determines the velocity field in the surroundings of the rotorcraft, including its interaction with the ground. An equation is added for the transport of a scalar that represents the density of dust, with appropriate source terms and boundary conditions that incorporate the physics of saltation. Saltation refers to the movement of fine particles along the surface that move in a series of irregular, discontinuous jumps under the influence of the flow. The transport of dust has been implemented in the code specifically for this work and allows to track the distribution and total mass of mobilized dust as a function of time in the simulations. This data is eventually compared with the observations.

This paper aims to investigate the potential for using data observed *in situ* on Mars to verify the implementation of numerical models for brownout. Specifically, a dedicated analysis of Ingenuity's flights by Lemmon et al. [14] has provided data on the mass of mobilized dust during several flight sequences. The mass has been estimated based on images recorded by the Perseverance rover with its cameras filming the helicopter and its environment. The images have been processed by comparing pixel brightness with a mean reference and relating changes in opacity to dust density. This dataset provides a unique opportunity to verify models against real world data in an extraterrestrial environment.

In this paper, we simulate the Ingenuity helicopter on Mars during IGE phases. We calculate the mass of dust mobilized for various parameters of the models and we compare our results with the observational data. Finally, we discuss the agreement and discrepancies in regard to the assumptions made in the numerical models and in the image processing technique.

III. Methods

A. Computational Fluid Dynamics Solver

The VPM method solves the Navier-Stokes equations in their vorticity-velocity formulation. It utilizes a hybrid Lagrangian-Eulerian discretization. On the one hand, vortex particles are employed to solve the flow advection. On the other hand, the stretching and diffusion are solved on a background Cartesian grid through the use of 4th-order finite differences. Sub-grid scale modeling is also performed by applying a filtering operation on the grid information. The resulting method is known to have low dissipation and dispersion errors [15], while being computationally efficient (including on massively parallel architectures) [16]. The aerodynamics of the wings and rotors are modeled using lifting lines which take care of shedding the appropriate vorticity in the vicinity of the lifting surfaces [17]. The ground is modeled as a flat surface accounted for in the simulation through a no-slip boundary condition on the Eulerian domain. This approach was verified against detached eddy simulation considering the flow around a single rotor in ground effect [18]. Additional comparisons with experimental and other numerical results showed favorable agreement. For conciseness, we refer to [16, 17, 19] for a detailed description of the method, and specifically to [20] for the description of the sub-grid scale model (also recently reviewed in [21]). Multiple rotorcraft applications have been explored with the VPM method [22–25, 25, 26], with consistent validation where possible. An example of a simulation of Ingenuity in hover above a flat ground is shown in Fig. 2.

For the purpose of this work, we introduce the capability for the model to compute the friction velocity at the wall. Assuming a smooth surface, we use the law of the wall by Reichardt [27],

$$u^+ = \frac{1}{\kappa}\log(1+\kappa y^+) + (C - \kappa\,\log(\kappa))(1 - e^{-y^+/11} - (y^+/11)\,e^{-y^+/3}), \tag{1}$$

with the conventional definition of wall variables $u^+ = {}^{u}/_{u_\tau}$ and $y^+ = {}^{(y\,u_\tau)}/_{\nu}$, and where the boundary layer parameters used in the following are the von Kármán constant $\kappa = 0.383$ and $C = 4.25$. The equation is solved for the friction velocity $u_\tau = \sqrt{\tau_{\mathrm{w}}/\rho}$. The value of u is set to the norm of the instantaneous velocity vector projected in a plane parallel to the ground at a given distance to the wall y, typically one grid point above the surface, assuming that this location is within the log region. This procedure is repeated for all grid points on the ground at every time step.

B. Helicopter Model

We developed a model of the Ingenuity helicopter for the VPM simulation environment. The model consists of two counter-rotating rotors with two blades each (Fig. 3). The blade planform geometry was taken from publicly available data [28, 29], and is shown in Fig. 4. We assumed all blades were made with the `CLF5605` airfoil along the entirety of their span. Since the aerodynamics of the blades are represented with a lifting line approach in the VPM simulations, we generated a full set of 2D polar data using XFOIL [30]. The lifting line is fed with the so-obtained lift and drag coefficients tabulated as a function of Reynolds and Mach numbers.

The simulations presented in this article were performed under Martian conditions. The corresponding environmental and rotor parameters are summarized in Tables 1 and 2. While the rotors' rotational speed was set to its nominal value, the collective pitch angle was manually adjusted so that the total thrust balances the weight of the vehicle (for a mass of 1.8kg).

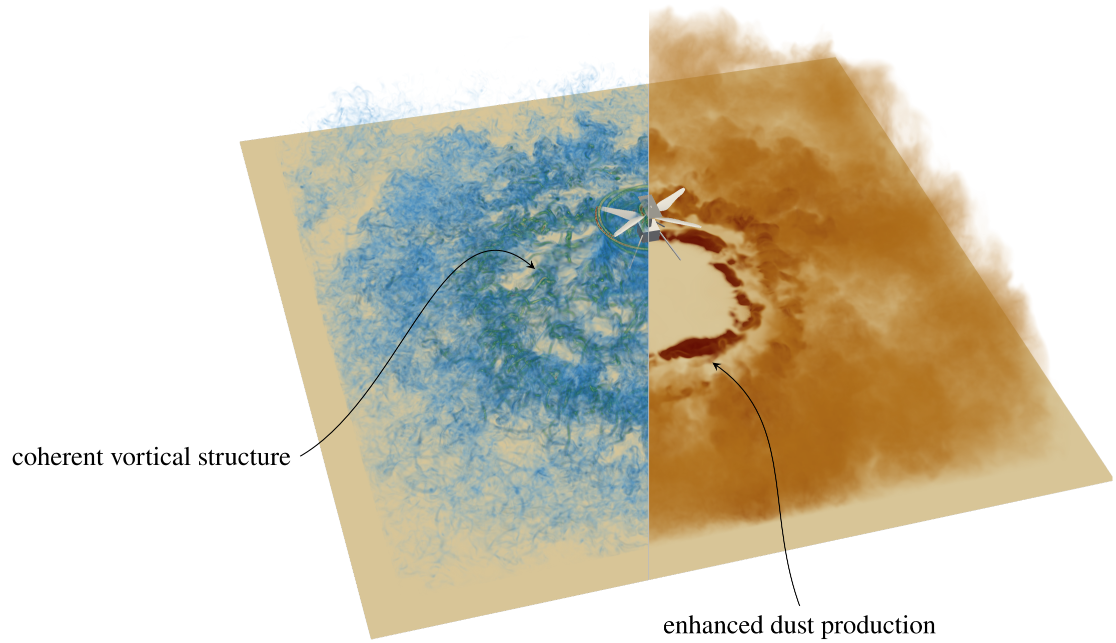

Fig. 2 Visualization of a snapshot result from the simulation of Ingenuity hovering at $h/R = 2$, showing the vorticity field on the left and the density of dust on the right, by volume rendering.

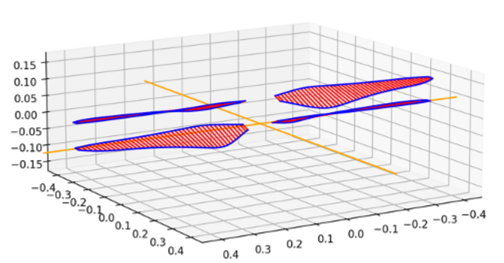

Fig. 3 3-D geometry of Ingenuity's rotors model.

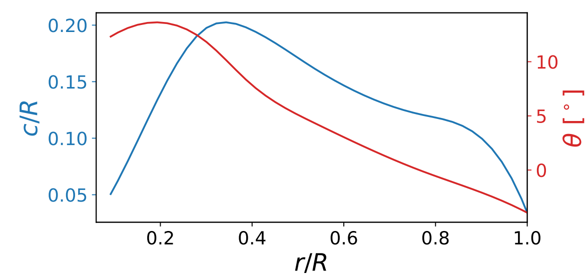

Fig. 4 Chord and twist distributions of the model.

C. 3-D Dust Mobilization Model

We support the derivation of Phillips and Brown [10] and all the assumptions involved to arrive at an equation for the transport of particulate matter with given particle properties, represented as a continuous phase of density ρ_p,

$$\frac{\partial \rho_\mathrm{p}}{\partial t} + (\mathbf{u} + \mathbf{u}_\mathrm{g}) \cdot \nabla \rho_\mathrm{p} = S_\mathrm{p} + D_\mathrm{pt} \nabla^2 \rho_\mathrm{p}, \tag{2}$$

with $\mathbf{u}$ the flow velocity, $\mathbf{u}_\mathrm{g}$ the particle fallout velocity, S_p a source term, and D_pt an effective mass diffusivity constant. The fallout velocity is modeled as in [10],

$$u_\mathrm{g} = \frac{\nu}{d} \left(\sqrt{25 + 1.2 d_\star} - 5 \right)^{1.5}, \tag{3}$$

where the dimensionless particle diameter is defined as $d_\star = d \left(g(\rho_\mathrm{s} - \rho)\rho^{-1}\nu^{-2} \right)^{1/3}$. The effective diffusivity is computed as $D_\mathrm{pt} = \nu_\mathrm{t}/\mathrm{Sc}_\mathrm{t} + D_\mathrm{p}$, where ν_t is the flow turbulent viscosity provided by the sub-grid scale model, Sc_t is the turbulent Schmidt number, and D_p is the molecular diffusivity. Our estimate for the latter is based on the Stokes-Einstein-Sutherland equation and suggests that it is negligible compared to the sub-grid scale contribution.

The entrainment of dust particles in the flow is modeled through S_p that is only active at the first grid point above the wall. The underlying physical process that we model is that of saltation. As reviewed in depth by Kok et al. [31], when saltation occurs, dust particles are mobilized in a rolling-hopping motion with a direction mostly parallel to the ground. The onset of the phenomenon depends on the balance between the gravity force, the aerodynamic drag, and the interparticle cohesion force acting on the particles. While saltation forms a thin layer of entrained dust above the ground surface, a fraction of the saltating particles is further entrained into the flow which then transports them away from the surface. The source term in Eq. (2) acts to capture this fraction of dust particles that are lifted from the ground after the velocity reaches the saltation threshold.

Two velocity thresholds are involved in the model, which we here assume to be fixed parameters. The first one is the saltation fluid threshold u_ft which characterizes the onset of saltation when lifting of a small number of particles occurs. The second one, the impact threshold u_it, parameterizes the smallest velocity at which saltation can be sustained after it has been initiated. On Mars, a typical value for the ratio $u_\mathrm{it}/u_\mathrm{ft}$ is 0.1 [31].

Correlations were developed from experimental data to quantify the horizontal flux of dust that enters in saltation. A widely accepted model [32, 33] is

$$Q = 2.61 \frac{\rho}{g} u_\tau^3 \left(1 - \frac{u_\mathrm{it}^3}{u_\tau^3}\right)\left(1 + \frac{u_\mathrm{it}}{u_\tau}\right). \tag{4}$$

The vertical flux of dust entering the flow is then calculated as

$$F = \alpha\, Q, \tag{5}$$

where α is commonly referred to as the sandblasting efficiency, and has units of m^{-1}. Finally, $S_\mathrm{p} = F/\Delta x$ is the source term in Eq. (2) since F is a mass flux per unit area and we rather impose it as a source term in the volume.

Regarding the estimation of mobilized dust, the total mass is calculated as the integral of the dust density in the whole computational domain,

$$M(t) = \int \rho_\mathrm{p}(\mathbf{x})\mathrm{d}\mathbf{x}. \tag{6}$$

The finiteness of the domain has implications on the computed mass that are discussed at the end of this paper. The simulations in this study assume a monodisperse particle field. The numerical values for the main model parameters are given in Table 3.

Table 1 Environmental properties.

$g =$	3.721	$\mathrm{m/s^2}$
$\rho =$	0.020	$\mathrm{kg/m^3}$
$\nu =$	5.65×10^{-4}	$\mathrm{m^2\,s^{-1}}$

Table 2 Rotor operating conditions.

$R =$	0.605	m
$b =$	0.073	m
$\Omega =$	2 500	RPM
$\theta_0 =$	4.0	°

Table 3 Dust properties.

$\rho_\mathrm{s} =$	2 000	$\mathrm{kg/m^3}$
$d =$	1.4	µm
$\mathrm{Sc_t} =$	10	–
$\lVert\mathbf{u}_\mathrm{g}\rVert =$	0.030	$\mathrm{m\,s^{-1}}$

IV. Outwash Velocity Induced by Ingenuity in Hover

When a rotorcraft hovers above a flat surface, the flow induced by the rotor(s) is redirected from downwash in the region right underneath the rotors to outwash along the surface. In the region directly above the surface, a so-called wall jet forms with a velocity mainly pointing along the outward radial direction. The velocity profile across the thickness of the jet has been measured experimentally for various model-scale and full-scale rotorcrafts on Earth (see, e.g., [34] and references therein). It has been shown that, when established, the jet adopts a self-similar profile that appears to be universal, where the similarity variables are u_max and $z_{1/2}$. The former is the maximum velocity in the jet, and the latter is the height at which the velocity reaches half of the maximum value. This self-similar behavior was also obtained in CFD simulations (see, e.g., our previous work [18]).

The time-averaged velocity profile in the jet is calculated for Ingenuity. The results are obtained from VPM simulations in a domain of size $6R \times 6R \times 6R$. A no-slip wall boundary condition is used to model the ground surface while all other boundaries are set to unbounded. The background Cartesian grid uses a uniform resolution corresponding to $\Delta x/R = 1/48$ unless otherwise specified. To simulate hover, the Ingenuity rotorcraft model is placed at a given height above the surface and at the center of the domain in the other two directions.

The resulting velocity profiles at a radial distance of $r/R = 1.5$ from the center of the rotors are shown in Figs. 5 and 6. In the former, the curves are normalized with rotor variables, where w is the far field rotor induced velocity (see also Section V.A). In the latter, the similarity variables are used. Increasing hover height leads to decreasing maximum velocity in the jet at a fixed radial location. On the other hand, the jet width increases until at least $h/R = 4$. The self-similar profile is observed for rotor heights under $r/R = 3.5$ but starts deviating as the rotor height further increases. Changes in $u_{\max}$ and $z_{1/2}$ are also quantified in Fig. 7.

To verify the consistency of the numerical modeling, the effect of the grid resolution on the calculated outwash velocity profile was evaluated. Three simulations of increasing resolutions were performed with $\Delta x/R = 1/24, 1/32$, and $1/48$. Results are shown in Fig. 8. The maximum velocity in the jet shows a converging behavior while $z_{1/2}$ also saturates. Even though only three resolutions are considered here, these results and previous experience with the code in similar configurations give us confidence in the consistency of the numerical modeling.

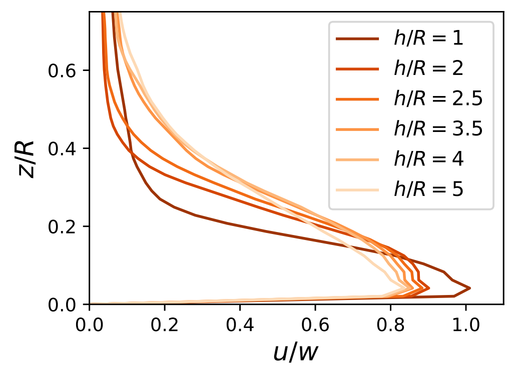

Fig. 5 Outwash velocity profile at a distance of $r/R = 1.5$ normalized with rotor variables.

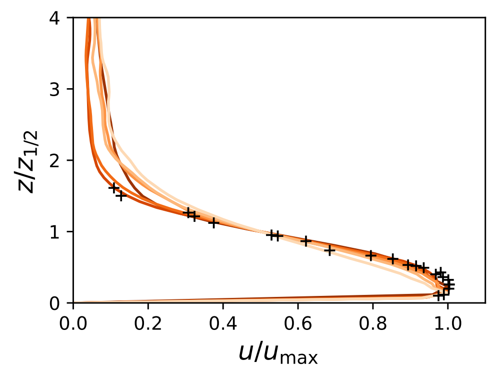

Fig. 6 Outwash velocity profile at a distance of $r/R = 1.5$ normalized with wall jet variables, overlayed with full-scale helicopter data (+) from [35].

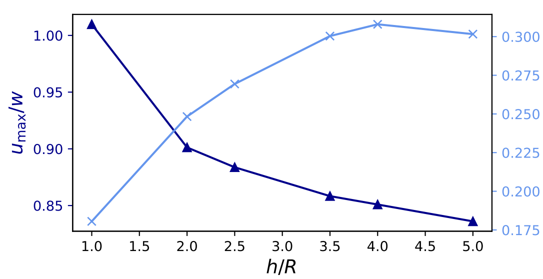

Fig. 7 Effect of height on the wall jet variables in the simulations of Ingenuity in hover ($\Delta x/R = 1/48$).

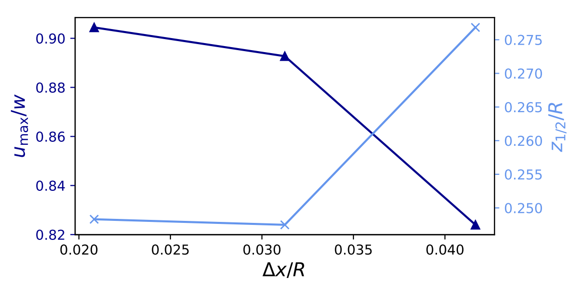

Fig. 8 Effect of grid resolution on the wall jet variables in the simulations of Ingenuity in hover at $h/R = 2$.

V. Friction Velocity on the Ground

The wall jet induced by the rotor causes friction on the ground surface. The friction velocity, a measure of the intensity of this effect, is a crucial quantity in the modeling of dust mobilization. As shown in Section III.C, the normal flux of dust mass at a given location on the surface scales with u_τ^3 when the friction velocity is above the flow threshold velocity. This section compares the values of u_τ calculated in the simulation with the predictions of an analytical model.

The numerical setup in this section is identical to the previous section. The friction velocity at every grid point on the ground surface is recorded during the simulations. The data collected during the first second (or equivalently, about 40 rotor revolution periods) is discarded to let the initial transient evacuate from the simulation domain and reach an established regime. Statistics are then collected over the following 2.5 s, that is, over about 100 rotor revolutions. The mean friction velocity is obtained by averaging over the azimuthal direction and time. Minimum and maximum u_τ

values encountered locally are also extracted from the same time interval. We compare these values with the prediction of the analytical model presented hereafter.

A. Rabinovitch Model and Comparison to Simulation Results

In computing the friction velocity, Lemmon et al. [14] use the model described by Rabinovitch et al. [8] which we recall here for completeness. This model predicts the wall shear stress τ_w as a function of the radial location from the impingement location by analogy with the analytic solution of an axisymmetric laminar stagnation flow,

$$\tau_\mathrm{w} = 1.3120\,\rho\,\nu^{1/2}\,a^{3/2}\,r, \tag{7}$$

where a is a parameter that represents a characteristic strain rate at the wall. The authors of the model propose to define the latter as

$$a_\mathrm{original} = \frac{w + u_\mathrm{tip\ vortex}}{2h}, \tag{8}$$

where $w = 2\sqrt{T/(2\rho A)}$ is the far-field rotor induced velocity from momentum theory with T the rotor thrust and A the rotor swept area. The strain rate includes a correction for the effect of tip vortices which locally increase the friction with an induced velocity estimated as $u_\mathrm{tip\ vortex} = 3.66T/(\sigma\rho A\Omega R)$, with σ the rotor solidity.

Since this model predicts that the shear stress increases monotonously with the radius from the stagnation point, a characteristic value is taken at the location $r/R = 1$ which is meant as a representative value for the shear stress induced by a rotorcraft on the ground. Let us note that this model does not account for unsteadiness and the intermittency of the friction induced by passing coherent vortical structures.

As an illustration, we compare the analytical prediction from Rabinovitch et al. [8] with the CFD-predicted friction velocity for Ingenuity's rotor system hovering at a height of two rotor radii. Figure 9 shows the friction velocity including mean, percentile, the envelope of the minimum and maximum values, and a sample instantaneous value. While the mean u_τ peaks at around $r/R = 1.5$, the 99.5^th percentile keeps growing until approximately $r/R = 1.8$ and then slowly decreases. This percentile value is here used as a representative value of the highest likely friction velocity as a function of the radius, since it is statistically more meaningful than the absolute maximum encountered in the simulation. Relatively large amplitude fluctuations arise from the instantaneous velocity field as illustrated by the instantaneous sample. The latter presents peaks and valleys associated with the passage of coherent vortical structures, also depicted in Fig. 2.

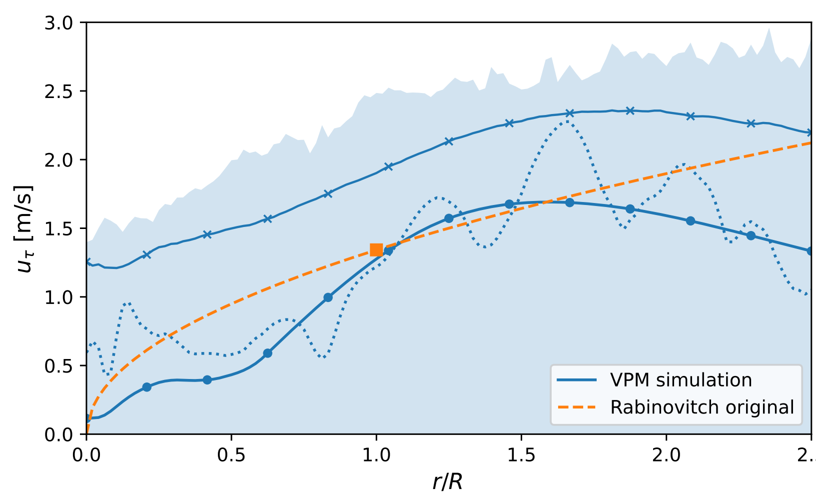

Fig. 9 Friction velocity on the ground simulated for Ingenuity hovering at $h/R = 2$ compared to the prediction of the original model by Rabinovitch et al. [8]. The time-averaged friction velocity (–●–), the 99.5^th percentile value (–×–), and a sample of the instantaneous signal (⋯) are shown. The area depicts the minimum and maximum values recorded for each radius.

The analytical model predicts a slightly lower friction velocity than the peak average u_τ calculated in the CFD. However, substantially higher friction velocities occur as illustrated by the 99.5$^{\text{th}}$ value which is about 1.5 times higher than the average.

Previous studies have suggested that dust kickups result from the action of local coherent flow features that are strong enough to entrain a significant amount of dust in the flow at once [11, 36]. As highlighted previously, such structures are indeed identified in the instantaneous u_τ sample and in the 3D vorticity and dust visualization (see also Section VI). For small helicopters, this mechanism drives the amount of dust entrained in the flow. Recent experimental evidence has suggested that coherent vortical structures such as tip vortices break down earlier in the wake of heavy rotorcraft on earth [37] —typically, before reaching the ground vicinity—, leaving an unresolved question as to the main source of dust kickups for these rotorcrafts. Regardless, it is desirable to predict the effect of more or less coherent turbulent structures on the time history of the friction velocity. To simplify the analysis as a starting point, we here focus on the 99.5$^{\text{th}}$ percentile friction velocity, a proxy for the higher u_τ Ingenuity is likely to generate as a function of its height. This quantity might be better suited to predict the onset of the brownout phenomenon since dust will start to be entrained in the flow as soon as the local friction velocity exceeds the fluid threshold velocity. We discuss this claim in Section VII.

B. Sensitivity to Rotor Height

To assess the sensitivity of the friction velocity to the rotor height, several simulations have been performed with Ingenuity hovering at various heights. The height is defined as the distance of the bottom rotor plane to the ground. The results are summarized in Fig. 10.

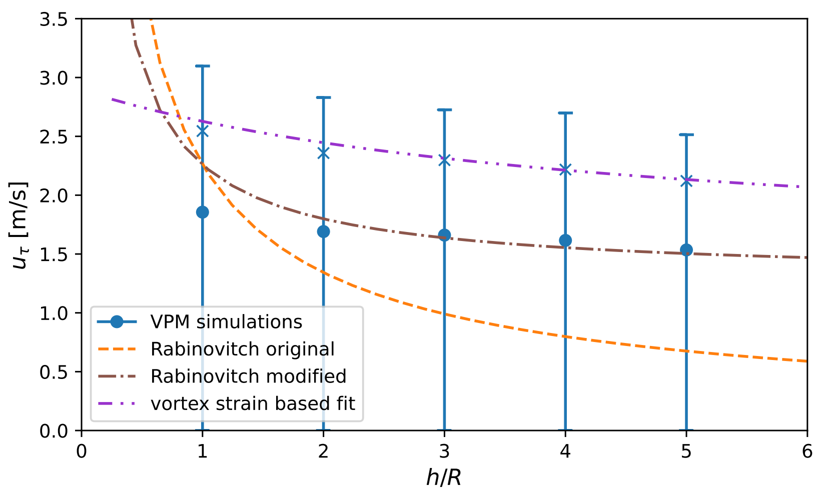

Fig. 10 Friction velocity on the ground predicted by the simulations of Ingenuity hovering at various heights. The displayed simulation results include the peak mean u_τ (—●—), the peak 99.5$^{\text{th}}$ percentile value (—×—). The height of the bar denotes the range between the overall minimum and maximum friction velocity recorded during the simulation. The model prediction by Rabinovitch et al.'s original model, our modified version, and a fit of the highest likely u_τ is also shown.

Both the peak 99.5$^{\text{th}}$ percentile (noted $u_\tau^{99.5^{\text{th}}\text{pct}}$ from here on) and the peak mean friction velocity exhibit a lower sensitivity to height compared to the original formulation of the analytic model. This can be problematic when one aims to use the analytic model to determine the flow threshold velocity from observational data, as proposed by Lemmon et al. [14].

We revisit the analytical model by Rabinovitch et al. [8] in light of these results. First, we note that a rotorcraft wake usually does not experience a significant expansion, as opposed to a regular jet. Instead, the area under the rotor where the induced velocity is significant remains relatively constant over a few radii under the rotor. It even contracts close to the rotor. While an expanding jet would induce a wall strain that decreases proportionally to the inverse of its height, we argue that the contribution of w to a should not. This motivates the modified expression:

$$a_{\text{modified}} = \frac{w}{2R} + \frac{u_{\text{tip vortex}}}{2h}. \tag{9}$$

On the other hand, the influence of the vortex-induced velocity still scales with the inverse of the height. Figure 10 shows the prediction of this modified model as a function of the rotor height. It better captures the trend in the peak mean friction velocity for heights above $h/R = 2$. However, the validity of this model would need to be evaluated on other rotorcrafts.

In addition, we are interested in modeling the maximum friction velocity. We propose to adapt again the expression of the strain rate to establish a fit of $u_\tau^{99.5^{\text{th}}\text{pct}}$ calculated in the simulation. When the wake ages, large coherent structures form as a result of the merging of blade tip vortices and subsequent vortex interactions. Since we postulate that the high friction velocity is caused by the passage of these structures, we define the new a as the strain induced by a coherent vortex at the location of its core radius σ_v:

$$a_{\text{fit}} = b_1 \frac{u_{\text{coherent vortex}}}{\sigma_v}, \tag{10}$$

where b_1 denotes a fitting parameter. We choose to model the vortex-induced velocity at the location of the core radius using the point vortex formulation,

$$u_{\text{coherent vortex}} = \frac{1}{2\pi} \frac{\Gamma_v}{\sigma_v}. \tag{11}$$

We model the circulation of the coherent structure as

$$\Gamma_v = \Gamma_0 \left(1 + \frac{1}{b_2} \frac{h}{w}\right), \tag{12}$$

where the initial circulation corresponds to the tip vortex circulation $\Gamma_0 = 2.3 \frac{w^2}{2} \frac{\bar{c}}{R\Omega\sigma}$, the same expression as in Rabinovitch et al.'s original model with $\bar{c}$ the blade mean chord and σ the rotor solidity. Equation (12) models the growth in circulation of the coherent structures as they merge with each other. The factor h/w represents the age of the structure when it reaches the vicinity of the ground, while b_2 (with units of seconds) is a fitting parameter to specify the time it takes for the structure to double in circulation. Finally, the growth in the average core size of the coherent structure is modeled as a typical vortex growth,

$$\sigma_v = \sqrt{r_0^2 + (4\alpha_L \nu_{\text{eff}}) \frac{h}{w}} \tag{13}$$

where $r_0 = 0.1\bar{c}$ is the assumed initial tip vortex core size, $\alpha_L = 1.25643$ is Lamb's constant, and ν_{eff} is an effective diffusivity. The latter is also a fitting parameter.

The result of the fit with parameters $b_1 = 0.22$, $b_2 = 0.25$ s, and $\nu_{\text{eff}} = 0.02$ m^2 s^{-1} is shown in Fig. 10. The fitted curve better captures the trend in $u_\tau^{99.5^{\text{th}}\text{pct}}$ compared to Rabinovitch et al.'s original or the modified models. However, from the engineering perspective, it is perhaps less valuable since the fitting parameters were not derived from rotor and operating quantities only. Hence, it cannot be directly applied to other rotorcraft if simulation or experimental data is not available.

VI. Lifted Dust during Take-Off

We focus on the total mass of dust mobilized during take-off of the Ingenuity rotorcraft. Our aim is to compare independent predictions of dust mobilization by the numerical simulations of this work and the dataset obtained by Lemmon et al. [14]. While the spatial distribution of dust would be hard to compare (even qualitatively) due to the limited resolution and the 2-D character of the images in the observations, a quantitative comparison is possible for the total mass of dust mobilized over time. This integral diagnostic allows a narrowed focus on the potential sources of discrepancy between the results of our numerical model and the data sourced in image processing. We identify three main quantities that significantly affect the dust model predictions: the friction velocity on the ground, the sandblasting efficiency which controls the vertical flux of dust, and the threshold velocities. This section illustrates the sensitivity of the mass of lifted dust to these three parameters.

Regarding the numerical setup, the flow is again initialized as quiescent and the counter-rotating rotors start spinning impulsively at their nominal rotational velocity at $t = 0$. We aim to emulate the take-off phase to match the configuration observed in reality. However, for simplicity, the kinematics of the vehicle are omitted. Instead, the rotorcraft is held at a fixed position in hover. The size of the domain is increased to $12R$ in the lateral directions while maintaining $6R$ vertically. To allow faster turnaround times, the simulations are run on a coarse mesh of resolution $\Delta x/R = 1/24$.

Due to the impulsive character of the start up in both the simulation and in reality, a starting vortex forms as a result of the merging of early tip vortices. As observed in Fig. 11, the starting vortex travels downwards and interacts with the dust on the surface. The wake then continues to entrain more particles from the ground, contributing to a growing cloud of dust. Around $t = 0.6$ s, some dust starts to exit the simulation domain under the effect of the rotor outwash velocity. Eventually, the simulation reaches an established condition in which dust is lifted from the ground, is entrained in the outwash flow, and eventually leaves the computational domain.

For the baseline case presented hereafter, the lower rotor is at a height of two rotor radii above the ground (as shown in Fig. 11). The sandblasting efficiency is set to $f = 0.004$ m^{-1}, the ratio $u_{\mathrm{it}}/u_{\mathrm{ft}}$ is assigned the value 0.1, and the threshold velocity $u_{\mathrm{ft}} = 0.54$ m s^{-1}. The latter is set to match the estimation by Lemmon et al. [14] from their observation combined with the original Rabinovitch model.

A. Effect of Sandblasting Efficiency

The vertical flux of mobilized dust, Eq. (5), drives the total amount of mobilized dust as it is directly proportional to the only source of dust in our model. Therefore, the sandblasting efficiency is a key parameter of the model that however incurs a high uncertainty. Indeed, various models have been proposed in the literature for α and their output may vary by several orders of magnitude. As an example, the model by Marticorena and Bergametti [38] leads to $\alpha = 0.00947$ m^{-1}

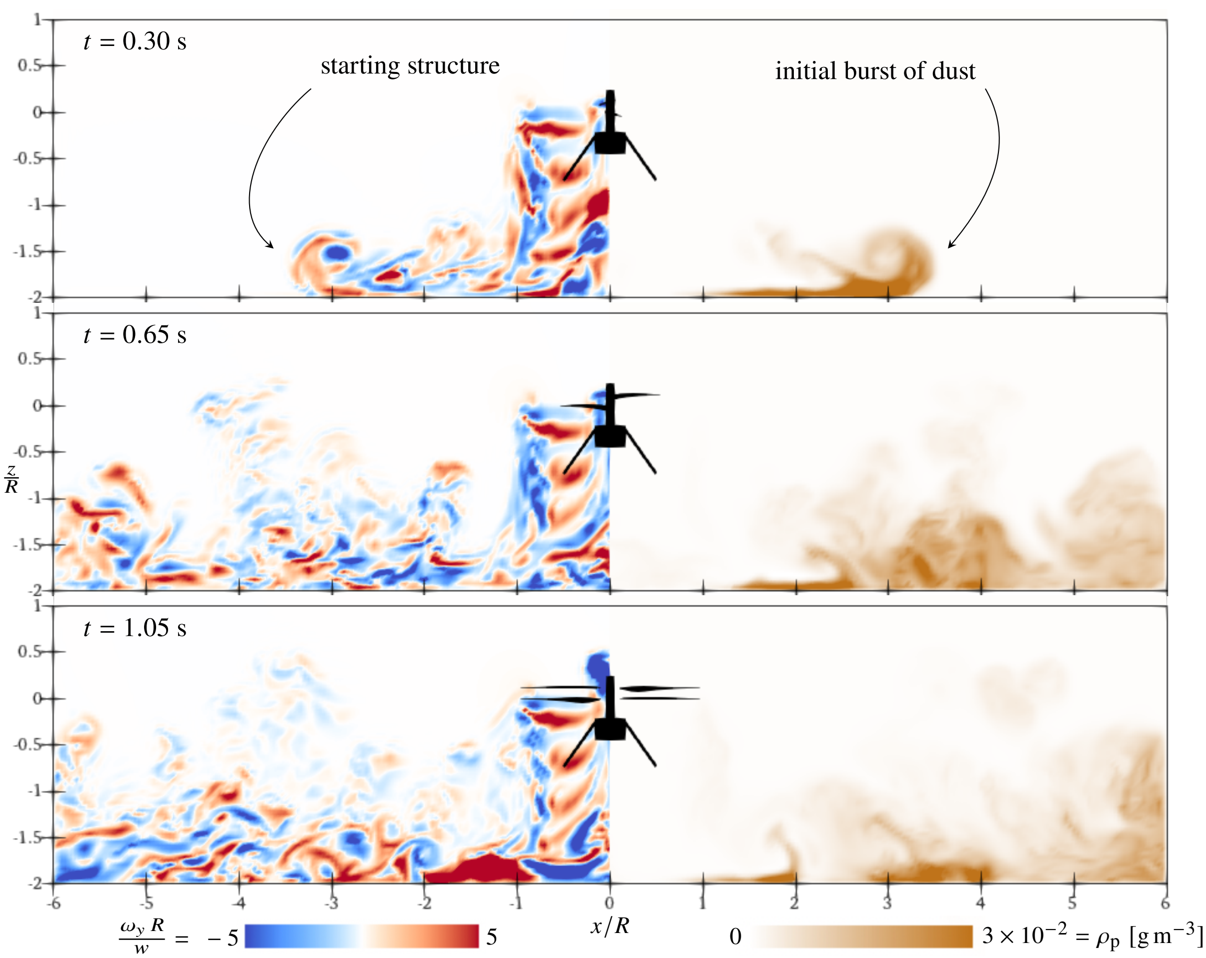

Fig. 11 Instantaneous snapshots of the plane-normal vorticity (left) and the density of dust (right) in a cross section of Ingenuity's simulation with $h/R = 2$ and $\Delta x/R = 1/24$.

for a soil clay content of 10% (as proposed by Phillips and Brown [10]). The model by Lu and Shao [39] includes more soil parameters but the output ranges between 10^2 and 10^4 for the assumed Martian conditions. In their study, Wu et al. [40] choose α freely. They also conclude that it might not be straightforward to port the sandblasting efficiency from one numerical implementation to another due to its sensitivity to unresolved surface layer processes.

To illustrate the effect of the sandblasting efficiency, we compute the mass of lifted dust is our simulations for various values of α, and we compare the results to Lemmon et al.'s processing output. The computed mass of dust mobilized during take-off is shown in Fig. 12 as a function of time.

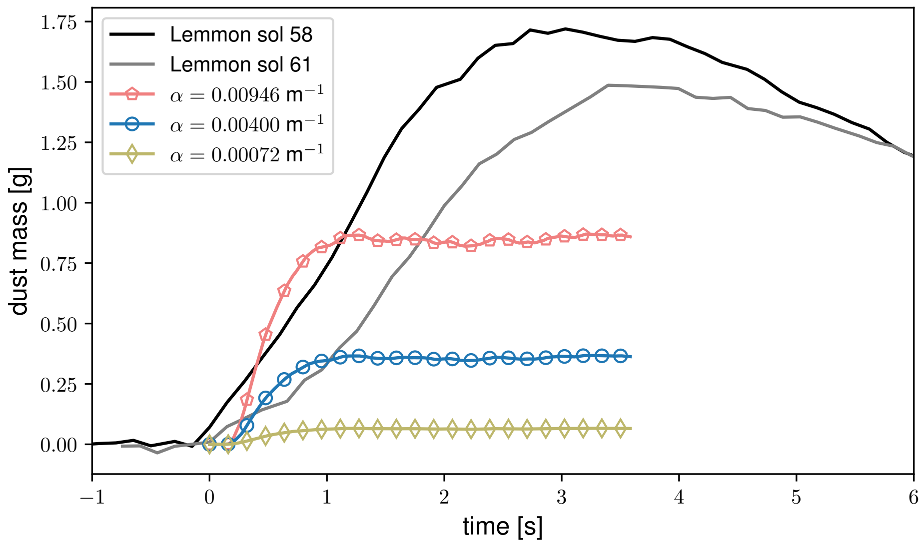

Fig. 12 Computed mass of mobilized dust as a function of time in the simulation compared to observational data from two different Martian sols. [14]

The mass of mobilized dust calculated in the simulation reflects the vortex dynamics of the impulsively started hovering rotor discussed above. In the initial phase, the mass grows rapidly under the effect of the starting structure that progressively covers a larger area until it reaches the domain boundary. The mass saturates after the starting vortex exited the domain and maintains itself at a relatively constant amount in the established phase. This amount is primarily a function of the size of the computational domain. This is an obvious limitation of our fixed size domain approach.

A similar behavior is seen in the data observed during the take-off of two different flights that Ingenuity performed on Martian sol 58 and sol 61. In these two instances, the rotorcraft ascends vertically up to a height of about 8 R (16 R, respectively) during the first 6 seconds (8 s, resp.) of the sequence and then maintains hover for at least 10 seconds. The initial phase is characterized by a growing cloud of dust the mass of which increases linearly over the first 1.5 to 2.0 seconds. The observed amount of dust then saturates as the cloud starts leaving the field of view of the camera. The observed mass then decreases as the cloud dissipates while Ingenuity is still in hover. Because it hovers at heights, the friction velocity associated with its wake at the end of the ascent is smaller than during the first instants of the take-off sequence. Dissipation and transport win over production which allows the total dust mass to decrease.

In the simulation results as well, the slope of the initial growth in dust mass is roughly linear and scales with the sandblasting efficiency. The total mass of dust in the established phase is proportional to α as expected. Considering the difference in size of the computational domain with respect to the field of view of the camera and the difference in the kinematics of the rotorcraft, it is meaningless to compare the mass of dust mobilized in the established phase between the observational and the simulation data. However, the parameters in the initial instants of the transient phase are similar enough to enable a more quantitative comparison of the lifted mass of dust and its rate. We note that, for the chosen values of u_{ft}, an α of about 0.004 m^{-1} gives a favorable agreement of the slopes. Going further than this simple argument based on orders of magnitude is complicated by the uncertainty on both u_{ft} and α. Therefore, we limit the scope of the rest of this work to sensitivity analyses of the numerical results to model parameters.

B. Effect of Threshold Velocities

We evaluate the effect of the fluid threshold velocity on the mass of mobilized dust. Threshold velocities are subject to a relatively large uncertainty because they depends on unmeasured soil properties for the observational data at hand. An additional source of discrepancy comes from modeling itself since various expressions and correlations have been proposed for both u_{ft} and u_{it} (as reviewed by Kok et al. [31]).

Considering Lemmon et al.'s estimation of $u_{\text{ft}} = 0.54\ \text{m s}^{-1}$ as the baseline, Fig. 13 shows that a threefold increase in u_{ft} leads to a threefold decrease in dust mass. However, a fourfold increase in u_{ft} leads to the almost complete suppression of the dust production at the wall. The total mass of dust is thus highly sensitive to the threshold velocity which, similarly to α, can cause orders of magnitude changes in the calculated value. It is therefore impossible to discriminate the effect of α and u_{ft} solely from the observed integrated mass of mobilized dust since both parameters can induce large variations on the result.

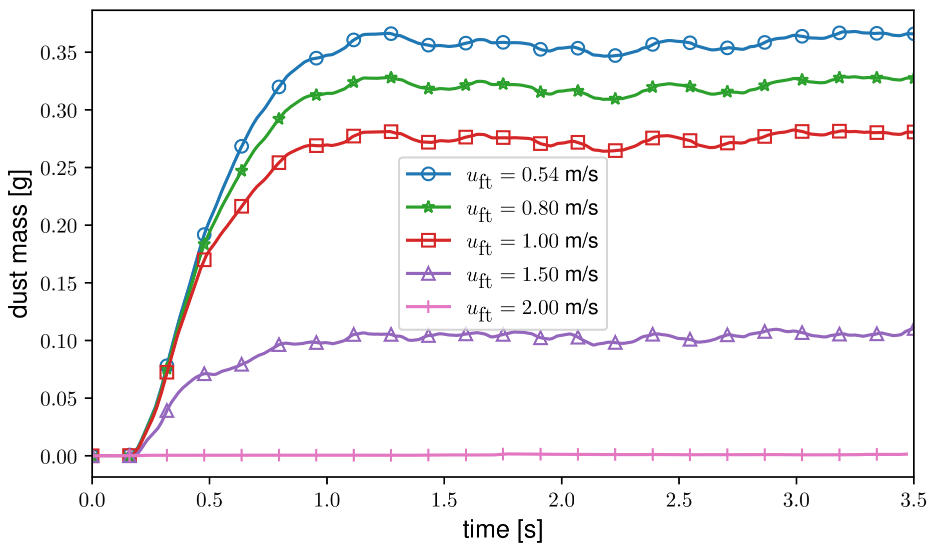

Fig. 13 Computed mass of mobilized dust as a function of time for various fluid threshold velocities.

However, if either of these parameters can be estimated separately within a certain degree of accuracy, the CFD results on dust mass could help reduce the uncertainty on the other. In fact, an independent method to estimate the threshold velocity was used by Lemmon et al.. The saltation flow threshold velocity was determined empirically from visual inspection of the video footage by noting the time when the cloud of dust started forming during landing sequences. Knowing the height of the rotorcraft at that time, u_{ft} was determined as the friction velocity calculated with Rabinovitch et al.'s original model at the corresponding altitude. The advantage of this approach is that it is completely independent of any assumption on the soil properties. The accuracy of the so-estimated u_{ft} mainly depends on the accuracy of the friction velocity model. On that note, the results presented in Section V.B suggest that the original model may have led to underestimated threshold velocities. If the estimation of u_{ft} from the video footages was repeated using the modified model instead, the threshold velocity would rather lie between 1.5 to $2.0\ \text{m s}^{-1}$.

Several sources in the literature report that the threshold velocity for a particle size of $d = 1.4\ \mu\text{m}$ (assumed here and by Lemmon et al.) is indeed higher than $0.54\ \text{m s}^{-1}$, by up to one order of magnitude (see [31, Fig.21(b)]). A threshold velocity of $u_{\text{ft}} \approx 1.5\ \text{m s}^{-1}$ could mean that the observed lifted particles were of a size 10 to 50 times bigger. Nevertheless, the outputs of existing models to calculate the threshold velocity of particles as a function of their size also range at least one order of magnitude. Even if the threshold velocity was determined very accurately from the empirical data (assuming there is no error in the friction velocity model), the size of the lifted particles could not be determined with certainty. Additionally, it is still unclear at this stage whether determining u_{ft} as described here based on a model of the peak average friction velocity is appropriate, considering the highly unsteady character of the velocity in the rotor-induced wall jet.

To conclude, it is desirable to further consolidate the estimation of the friction and threshold velocities as the CFD results could then help reduce the uncertainty on the sandblasting efficiency. Such an insight could help deduce useful information about the soil properties at the location where the rotorcraft operates.

C. Effect of Height

The sensitivity of the amount of dust lifted in the computational domain is assessed with respect to changes in rotorcraft heights for a given threshold velocity of $u_{ft} = 0.54$ m s^{-1}. From the implemented dust lifting model, we expect it to primarily depend on the value of u_τ through the definition of Q (Eq. (4)), and the ground area where the saltation criterion $u_\tau > u_{ft}$ is satisfied.

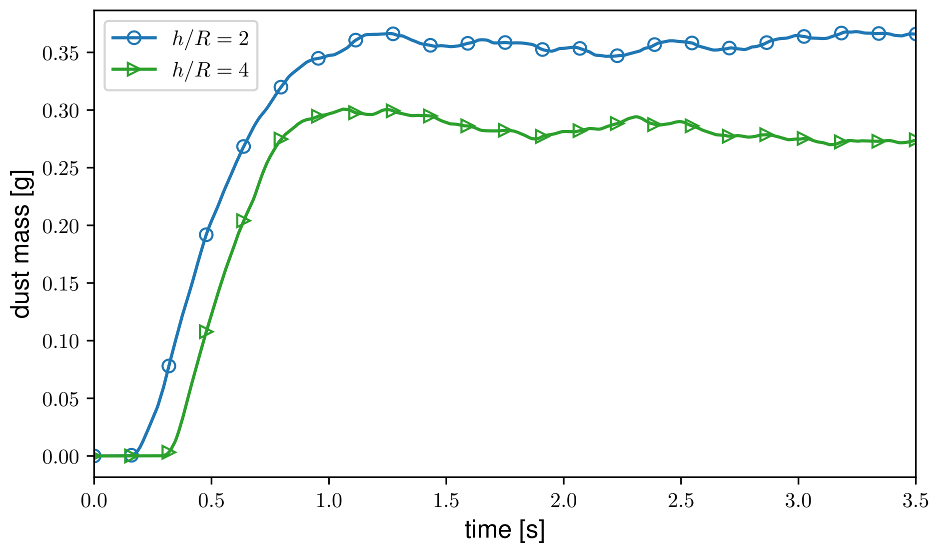

Fig. 14 Computed mass of mobilized dust as a function of time for various rotorcraft heights.

Figure 14 shows the mass of dust lifted in the simulation as a function of time for Ingenuity hovering at two different heights. On the one hand, the initial increase in dust mass has a very similar slope for both heights. This is another indication that the starting vortex structure drives the initial rate of dust production during the transient, considering that it has a similar circulation and structure in both cases.

On the other hand, the mass of mobilized dust in the established regime exhibits a sensitivity to rotor height, as expected. In this configuration, the simulations reveal that the peak average u_τ drops by approximately 5% between $h/R = 2$ and 4. This corresponds to a change in Q of -15%, everything else being kept constant. Yet, the mass of mobilized dust decreases by more than 22%, based on the average of the values presented in Fig. 14 over the last 1.5 s. The difference is due to the area where the saltation criterion is met which decreases when the hover height increases. Although these numbers need to be consolidated, the simulations confirm that tha mass of mobilized dust is not simply proportional to Q, nor is it proportional to u_τ. It is also possible that the degree of coherence of the vortical structures that reach the ground vicinity affects the efficiency of the dust-lifting mechanism. Finer simulations that can more accurately capture the flow features close to the ground are needed to examine this supposition.

VII. Discussion

Many assumptions have been made in the simulation and modeling framework presented here, as well as in the image processing by Lemmon et al.. This limits the representativeness of both datasets compared to the reality on Mars, as well as the scope of the comparison that can be made between them.

Among assumptions that are common between observations and simulations but differ from the actual Martian environment, the particulate matter considered was assumed to be monodisperse, from a single homogeneous specie. In reality, dust is better represented with a distribution of size and species with different characteristics. Furthermore, saltation was assumed to be the principal mechanism acting to lift dust in the atmosphere. As highlighted by Lemmon et al., direct aerodynamic lifting of particles or other processes associated with aggregates likely play a role.

As valuable as they are, the empirical data were obtained outside of the controlled environment of a laboratory. Virtually all environmental factors present uncertainty: wind conditions, variation in density of either the solid particles or the atmosphere, soil properties, wall roughness, etc. Additionally, the numerical values of the dust mass were obtained through image processing which further introduces its own constraints.

On the simulation side, one of the strongest assumptions made was to neglect the rotorcraft dynamics. Lemmon et al. mention thrust excursions of more than 20% compared to the nominal value that were necessary to execute commands or adjust to gusts. This should be accounted for to improve the consistency between the CFD and the observations. However, the data on the rotorcraft position, acceleration, and control inputs, is currently not publicly available. In any case, validity of the calculated mass of dust is limited by the size of the computational domain which remains smaller than the field of view of the camera in the observations. Also, possible depletion of particles on the ground as they get washed away was not accounted for.

Additional parameters would need to be better known to improve the accuracy of the numerical model. The effect of the impact threshold velocity was not discussed. From preliminary tests, the turbulent Schmidt number appeared to play a significant role in the calculated mass of mobilized dust. However, we could not find a readily available value in the literature for such a parameter. Let us also note that the accuracy of the friction velocity obtained from the CFD is contigent upon the capacity of the simulation to resolve the flow in the vicinity of the wall. In the present work, the simulation relied on a simplified representation of the wall that has shown favorable agreement with numerical and experimental velocity profiles in the outwash of a rotorcraft. Still, before drawing any definitive conclusion, we recommend that the results presented here be consolidated by comparison with other numerical method's predictions based on properly wall-resolved or wall-modeled schemes.

From the engineering perspective, it could be useful to derive a model of the dust production based on a characteristic friction velocity induced by the rotor and the related saltation fluxes. The results of this work showed that a characteristic area where the saltation criterion is active would need to be factored in in such a model. Nevertheless, it is unclear what value should be used for either of these. We have suggested to use the peak average u_τ for the former, although it is unclear whether this is sufficient to represent a quantity that is inherently stochastic. Additional efforts are needed to derive and validate an appropriate engineering model.

Finally, when it comes to comparing numerical and observational data, it should be mentioned that take-off and landing phases are quite different. The results from one should not be interchangeably used with the other. During take-off, it is suggested that the amount of lifted dust primarily depends on the development of the starting vortex which is associated with higher circulation and induced velocity. On the other hand, landing conditions are closer to established hover if the rotorcraft approaches the ground slowly. In Section V, the initial transient was explicitly removed from the simulation results in order to focus on the established regime. On the other hand, the comparison presented in Section VI focused exclusively on the transient phase because the amount of dust tracked in the simulation and visible in the observation are compatible only during the first instants of the flight. Nevertheless, there is an opportunity to extend the comparisons to the landing phase, although this would require larger computational domains in order to cover a wider area and track a more significant amount of dust. To account for potential errors arising from the image processing, a similar technique could also be applied to the numerical results to backsolve the opacity perceived by the sensor. Due to time constraints, this is left for future work.

VIII. Conclusions

The objectives of this research were to showcase the efficacy of modern numerical models to simulate brownout on other planets by comparison with Lemmon et al.'s dataset. Despite undeniably strong assumptions made in the simulation model as well as in the observational data processing, we reach the following conclusions:

- Critical environmental parameters driving the amount of dust lifted up during the simulation have been identified: the friction velocity at the wall, the saltation threshold velocities (u_{it},u_{ft}), and the sandblasting efficiency.
- Among these, the numerical simulation is most valuable in reducing the uncertainty on the friction velocity.
- The simulation results suggested that the sensitivity of the friction velocity with the height of the rotorcraft may have been overestimated in existing analytical models. A modified model as well as a fit of the peak 99.5$^{\mathrm{th}}$ percentile have been presented.
- When comparing the calculated and the empirically-derived mass of mobilized dust, it is virtually impossible to discriminate the effect of the saltation threshold velocity versus the sandblasting efficiency. Both parameters

depend on soil properties that are not easily determined or measured. Additionally, they suffer from modeling uncertainty that leads to orders of magnitude variations of the computed mass of dust. However, reducing the uncertainty in either of the parameters could help provide insights on the other.
- For a set of arbitrarily chosen environmental parameters, the results from the simulations emulating take-off suggested that the rate of production of mobilized dust primarily depends on the development of the starting vortex emanating from the impulsively started rotors. In the established regime, the numerical results corroborated that the mass of mobilized dust does not only depend on the flux of dust at the wall based on some characteristic friction velocity. The area where the saltation criterion is active must also play a role, as may other details of the local vortex dynamics.

Although its usability is hampered by inherent uncertainty, the data derived from Ingenuity's observations provided a wealth of information that still has secrets to unveil. Beyond that, Ingenuity's unprecedented achievements certainly paved the way for future exploration missions on extraterrestrial worlds.

IX. Acknowledgments

D.-G. Caprace is supported by an appointment to the NASA Postdoctoral Program at the NASA Ames Research Center, administered by Oak Ridge Associated Universities under contract with NASA. P. Ventura Diaz is supported by the Revolutionary Vertical Lift Technology (RVLT) Project. Resources supporting this work were provided by the NASA High-End Computing (HEC) Program through the NASA Advanced Supercomputing (NAS) Division at NASA Ames Research Center. The authors express their deep gratitude to Profs. Philippe Chatelain and Grégoire Winckelmans (UCLouvain, Belgium) for providing access to the source code of VPM4x.

References

[1] Young, L. A., Chen, R. T., Aiken, E. W., and Briggs, G. A., "Design opportunities and challenges in the development of vertical lift planetary aerial vehicles," *American Helicopter Society (AHS) Vertical Lift Aircraft Design Conference*, San Francisco, CA, 2000.

[2] Dull, C., Wagner, L., Young, L., and Johnson, W., "Hover and forward flight performance modeling of the Ingenuity Mars Helicopter," *Aeromechanics for Advanced Vertical Flight Technical Meeting, Transformative Vertical Flight*, edited by American Helicopter Society, San Jose, CA, 2022.

[3] Young, L., Aiken, E., Lee, P., and Briggs, G., "Mars rotorcraft: possibilities, limitations, and implications for human/robotic exploration," *2005 IEEE Aerospace Conference*, 2005, pp. 300–318. https://doi.org/10.1109/AERO.2005.1559324.

[4] Young, L. A., Delaune, J., Johnson, W., Withrow, S., Cummings, H., Sklyanskiy, E., Izraelevitz, J., Schutte, A., Fraeman, A., and Bhagwat, R., "Design Considerations for a Mars Highland Helicopter," *ASCEND 2020*, virtual, 2020. https://doi.org/10.2514/6.2020-4027, URL https://arc.aiaa.org/doi/abs/10.2514/6.2020-4027.

[5] Rutter, C., and Lach, M., "Feasibility Study of a Robotic Science Arm on Future Martian Rotorcraft," *Aeromechanics for Advanced Vertical Flight Technical Meeting, Transformative Vertical Flight*, edited by American Helicopter Society, San Jose, CA, 2022.

[6] Anderson, J. L., Karras, J. T., Cacan, M., Kubiak, G., Pyrzak, G., Dor, H., and Pipenberg, B., "Ingenuity, One Year of Flying on Mars," *IEEE Aerospace Conference*, 2023, pp. 1–18. https://doi.org/10.1109/AERO55745.2023.10115837.

[7] Lorenz, R. D., "Triboelectric Charging and Brownout Hazard Evaluation for a Planetary Rotorcraft," *AIAA AVIATION 2020 FORUM*, 2020. https://doi.org/10.2514/6.2020-2837.

[8] Rabinovitch, J., Lorenz, R., Slimko, E., and Wang, K.-S. C., "Scaling sediment mobilization beneath rotorcraft for Titan and Mars," *Aeolian Research*, Vol. 48, 2021, p. 100653. https://doi.org/10.1016/j.aeolia.2020.100653.

[9] Lorenz, R. D., "Sand Transport on Titan: A Sticky Problem," *Geophysical Research Letters*, Vol. 49, No. 10, 2022, p. e2022GL098375. https://doi.org/10.1029/2022GL098375.

[10] Phillips, C., and Brown, R. E., "Eulerian Simulation of the Fluid Dynamics of Helicopter Brownout," *Journal of Aircraft*, Vol. 46, No. 4, 2009, pp. 1416–1429. https://doi.org/10.2514/1.41999.

[11] Phillips, C., Kim, H. W., and Brown, R. E., "The flow physics of helicopter brownout," *66th AHS Forum: Rising to New Heights in Vertical Lift Technology*, edited by American Helicopter Society, Phoenix, AZ, 2010. URL https://strathprints.strath.ac.uk/27362/.

[12] Tan, J. F., er Gao, J., Barakos, G. N., Lin, C. L., Zhang, W. G., and Huang, M. Q., "Novel approach to helicopter brownout based on vortex and discrete element methods," *Aerospace Science and Technology*, Vol. 116, 2021, p. 106839. https://doi.org/doi.org/10.1016/j.ast.2021.106839.

[13] Rovere, F., Barakos, G. N., and Steijl, R., "Comparison between Eulerian and Lagrangian methods to predict brownout clouds," *Aerospace Science and Technology*, Vol. 137, 2023, p. 108306. https://doi.org/10.1016/j.ast.2023.108306.

[14] Lemmon, M. T., Lorenz, R. D., Rabinovitch, J., Newman, C. E., Williams, N. R., Sullivan, R., Golombek, M. P., Bell III, J. F., Maki, J. N., and Vicente-Retortillo, A., "Lifting and Transport of Martian Dust by the Ingenuity Helicopter Rotor Downwash as Observed by High-Speed Imaging From the Perseverance Rover," *Journal of Geophysical Research: Planets*, Vol. 127, No. 12, 2022, p. e2022JE007605. https://doi.org/10.1029/2022JE007605.

[15] Winckelmans, G., Cocle, R., Dufresne, L., and Capart, R., "Vortex methods and their application to trailing wake vortex simulations," *C. R. Phys.*, Vol. 6, No. 4-5, 2005, pp. 467–486. https://doi.org/10.1016/j.crhy.2005.05.001.

[16] Chatelain, P., Curioni, A., Bergdorf, M., Rossinelli, D., Andreoni, W., and Koumoutsakos, P., "Billion vortex particle Direct Numerical Simulations of aircraft wakes," *Computer Methods in Applied Mechanics and Engineering*, Vol. 197, No. 13, 2008, pp. 1296–1304. https://doi.org/10.1016/j.cma.2007.11.016.

[17] Caprace, D.-G., Winckelmans, G., and Chatelain, P., "An immersed lifting and dragging line model for the vortex particle-mesh method," *Theoretical and Computational Fluid Dynamics*, Vol. 34, 2020, pp. 21–48. https://doi.org/10.1007/s00162-019-00510-1.

[18] Caprace, D.-G., Ventura Diaz, P., and Yoon, S., "Simulation of the Rotorwash Induced by a Quadrotor Urban Air Taxi in Ground Effect," *79th VFS annual forum*, edited by V. F. Society, West Palm Beach, Florida, 2023.

[19] Mimeau, C., and Mortazavi, I., "A Review of Vortex Methods and Their Applications: From Creation to Recent Advances," *Fluids*, Vol. 6, No. 2, 2021. https://doi.org/10.3390/fluids6020068, URL https://www.mdpi.com/2311-5521/6/2/68.

[20] Jeanmart, H., and Winckelmans, G., "Investigation of eddy-viscosity models modified using discrete filters: A simplified regularized variational multiscale model and an enhanced field model," *Physics of Fluids*, Vol. 19, No. 5, 2007, p. 055110. https://doi.org/10.1063/1.2728935.

[21] de Crouy-Chanel, M., Mimeau, C., Mortazavi, I., Mariotti, A., and Salvetti, M. V., "Large-Eddy Simulations with remeshed Vortex methods: An assessment and calibration of subgrid-scale models," *Computers & Fluids*, Vol. 277, 2024, p. 106287. https://doi.org/10.1016/j.compfluid.2024.106287.

[22] Caprace, D.-G., Chatelain, P., and Winckelmans, G., "Wakes of rotorcraft in advancing flight: A large eddy simulation study," *Physics of Fluids*, Vol. 32, No. 8, 2020, p. 087107. https://doi.org/10.1063/5.0015162.

[23] Caprace, D.-G., Winckelmans, G., and Chatelain, P., "Assessment of the Vortex Particle-Mesh Method for Efficient LES of Hovering Rotors and their Wakes," *AIAA Scitech 2021 Forum*, 2021. https://doi.org/10.2514/6.2021-0738.

[24] Caprace, D.-G., Ning, A., Chatelain, P., and Winckelmans, G., "Effects of rotor-airframe interaction on the aeromechanics and wake of a quadcopter in forward flight," *Aerospace Science and Technology*, 2022, p. 107899. https://doi.org/10.1016/j.ast.2022.107899, URL https://www.sciencedirect.com/science/article/pii/S1270963822005739.

[25] Caprace, D.-G., and Ning, A., "Large Eddy Simulation for Empirical Modeling of the Wake of Three Urban Air Mobility Vehicles," *Journal of the American Helicopter Society*, Vol. 64, No. 4, 2023, pp. pp. 42002–42017(16). https://doi.org/10.4050/JAHS.68.042002.

[26] Caprace, D.-G., Diaz, P. V., and Yoon, S., "Simulation of a Single Rotor and a Quadrotor Hovering in Full and Partial Ground Effect," *AIAA AVIATION 2023 Forum*, San Diego, CA, 2023. https://doi.org/10.2514/6.2023-4281, URL https://arc.aiaa.org/doi/abs/10.2514/6.2023-4281.

[27] Reichardt, H., "Vollständige Darstellung der turbulenten Geschwindigkeitsverteilung in glatten Leitungen," *ZAMM - Journal of Applied Mathematics and Mechanics / Zeitschrift für Angewandte Mathematik und Mechanik*, Vol. 31, No. 7, 1951, pp. 208–219. https://doi.org/10.1002/zamm.19510310704.

[28] Koning, W. J., Johnson, W., and Allan, B. G., "Generation of mars helicopter rotor model for comprehensive analyses," *AHS Specialists' Conference on Aeromechanics Design for Transformative Vertical Flight*, edited by American Helicopter Society, San Jose, CA, 2018.

[29] Pipenberg, B. T., Keennon, M., Tyler, J., Hibbs, B., Langberg, S., Balaram, J. B., Grip, H. F., and Pempejian, J., "Design and Fabrication of the Mars Helicopter Rotor, Airframe, and Landing Gear Systems," *AIAA Scitech 2019 Forum*, 2019. https://doi.org/10.2514/6.2019-0620, URL https://arc.aiaa.org/doi/abs/10.2514/6.2019-0620.

[30] Drela, M., "XFOIL: An analysis and design system for low Reynolds number airfoils," *Low Reynolds number aerodynamics*, Springer, 1989, pp. 1–12. https://doi.org/10.1007/978-3-642-84010-4_1.

[31] Kok, J. F., Parteli, E. J. R., Michaels, T. I., and Karam, D. B., "The physics of wind-blown sand and dust," *Reports on Progress in Physics*, Vol. 75, No. 10, 2012, p. 106901. https://doi.org/10.1088/0034-4885/75/10/106901.

[32] Kawamura, R., "Study of sand movement by wind," Tech. Rep. Translated (1965) as Report HEL 2–8, University of California Hydraulics Engineering Laboratory, Berkeley, 1951.

[33] White, B. R., "soil transport by winds on Mars," *Journal of Geophysical Research: Solid Earth*, Vol. 84, No. B9, 1979, pp. 4643–4651. https://doi.org/10.1029/JB084iB09p04643.

[34] Ramasamy, M., and Yamauchi, G. K., "Using Model-Scale Tandem-Rotor Measurements in Ground Effect to Understand Full-Scale CH-47D Outwash," *Journal of the American Helicopter Society*, Vol. 62, No. 1, 2017, pp. 1–14. https://doi.org/10.4050/JAHS.62.012004.

[35] Silva, M., and Riser, R., "CH-47D tandem rotor outwash survey," *67th Annual Forum of the American Helicopter Society*, edited by American Helicopter Society, Virginia Beach, VA, 2011.

[36] Thomas, S., Lakshminarayan, V. K., Kalra, T. S., and Baeder, J. D., "Eulerian-Lagrangian analysis of cloud evolution using CFD coupled with a sediment tracking algorithm," *67th Annual Forum of the American Helicopter Society*, edited by American Helicopter Society, Virginia Beach, VA, 2011.

[37] Braukmann, J. N., Schwarz, C., Wolf, C., Buron, E., Koch, S., Buske, G., and Gardner, A., "BOS and Hot-Film Analysis of a CH-53G Helicopter Wake in Ground Effect," *79th Vertical Flight Society Annual Forum and Technology Display*, edited by American Helicopter Society, 2023, pp. 1–15.

[38] Marticorena, B., and Bergametti, G., "Modeling the atmospheric dust cycle: 1. Design of a soil-derived dust emission scheme," *Journal of Geophysical Research: Atmospheres*, Vol. 100, No. D8, 1995, pp. 16415–16430. https://doi.org/10.1029/95JD00690.

[39] Lu, H., and Shao, Y., "Toward quantitative prediction of dust storms: an integrated wind erosion modelling system and its applications," *Environmental Modelling & Software*, Vol. 16, No. 3, 2001, pp. 233–249. https://doi.org/10.1016/S1364-8152(00)00083-9.

[40] Wu, Z., Richardson, M. I., Zhang, X., Cui, J., Heavens, N. G., Lee, C., Li, T., Lian, Y., Newman, C. E., Soto, A., Temel, O., Toigo, A. D., and Witek, M., "Large Eddy Simulations of the Dusty Martian Convective Boundary Layer With MarsWRF," *Journal of Geophysical Research: Planets*, Vol. 126, No. 9, 2021, p. e2020JE006752. https://doi.org/10.1029/2020JE006752.